IOP Publishing Journal of Physics: Condensed Matter
J. Phys.: Condens. Matter **28** (2016) 344005 (8pp) doi:10.1088/0953-8984/28/34/344005

The ion dependence of carbohydrate binding of CBM36: an MD and 3D-RISM study

Shoichi Tanimoto[1], Masahiro Higashi[2], Norio Yoshida[1] and Haruyuki Nakano[1]

[1] Department of Chemistry, Graduate School of Science, Kyushu University, 744 Motooka, Nishi-ku, Fukuoka 819-0395, Japan
[2] Department of Chemistry, Biology and Marine Science, University of the Ryukyus, 1 Senbaru, Nishihara, Okinawa 903-0213, Japan

E-mail: higashi@sci.u-ryukyu.ac.jp and noriwo@chem.kyushu-univ.jp

Received 7 April 2016, revised 6 May 2016
Accepted for publication 16 May 2016
Published 1 July 2016

Abstract

The molecular recognition process of the carbohydrate-binding module family 36 (CBM36) was examined theoretically. The mechanism of xylan binding by CBM36 and the role of Ca^{2+} were investigated by the combined use of molecular dynamics simulations and the 3D reference interaction site model method. The CBM36 showed affinity for xylan after Ca^{2+} binding, but not after Mg^{2+} binding. Free-energy component analysis of the xylan-binding process revealed that the major factor for xylan-binding affinity is the electrostatic interaction between the Ca^{2+} and the hydroxyl oxygens of xylan. The van der Waals interaction between the hydrophobic side chain of CBM36 and the glucopyranose ring of xylan also contributes to the stabilization of the xylan-binding state. Dehydration on the formation of the complex has the opposite effect on these interactions. The affinity of CBM36 for xylan results from a balance of the interactions between the binding ion and solvents, hydrophilic residues around xylan, and the hydroxyl oxygens of xylan. When CBM binds Ca^{2+}, these interactions are well balanced; in contrast, when CBM binds Mg^{2+}, the dehydration penalty is excessively large.

Keywords: carbohydrate-binding module, molecular recognition, solvation effect, molecular dynamics simulation, 3D-RISM

(Some figures may appear in colour only in the online journal)

1. Introduction

Glycoside hydrolases from microorganisms play a major role in degrading plant cell walls, which account for a large part of the biological resources on the earth. The hydrolases have a characteristic multimodular architecture [1, 2]. Typical bacterial enzymes include at least one catalytic module and several ancillary modules. Some ancillary modules function to recognize and bind carbohydrates, such as cellulose, xylan, chitin, and pectin, in addition to their hydrolysis function. These are called carbohydrate-binding modules (CBMs). Binding of polysaccharides by the CBMs enhances the hydrolytic activity of enzymes although CBMs themselves do not have a hydrolytic function [3, 4]. Furthermore, it is considered that the binding process of CBMs is the initial and rate-determining process of the carbohydrate degradation reaction. However, the mechanism of the carbohydrate binding remains unclear [5].

Since the first discovery of CBMs in 1986, many investigators have sought to unravel the molecular details of selective carbohydrate binding and the structures of CBMs, mainly using nuclear magnetic resonance (NMR) spectroscopy and x-ray crystal structure analysis [6]. For example, the binding site of CBM1, from *Hypocrea jecorina*, was elucidated by NMR spectroscopy [7], and the topography and the binding properties of CBM29, from *Piromyces equi* and CBM6

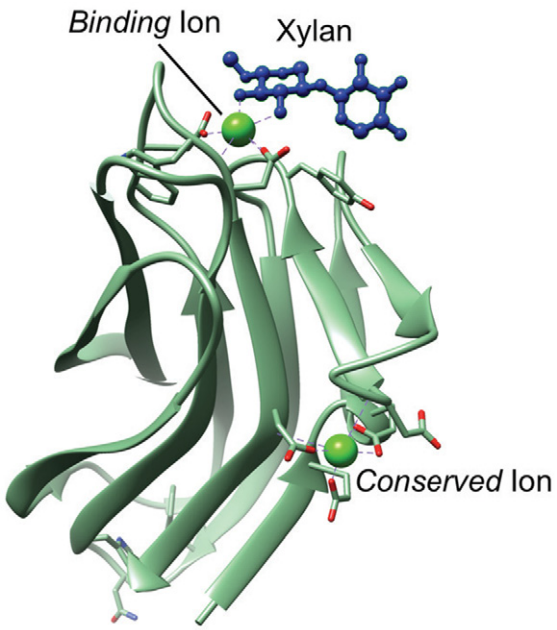

Figure 1. Overview of the CBM36 structure taken from Protein Data Bank entry ID 1ux7.

from *Bacillus halodurans* were elucidated by x-ray crystal structure analysis [8, 9]. Currently, through these and many other investigations, CBMs have been classified into more than 70 families and three binding types [10]. Type A CBMs have a hydrophobic planar surface comprising aromatic residues that bind crystalline substrates; type B CBMs have open clefts that accommodate polysaccharides; and type C CBMs have the lectin-like properties, which have structural similarity to the type B CBMs, but bind smaller saccharides in surface pocket indentations.

CBM36 is a novel CBM family. It has the unique and attractive property of being able to bind xylan preferentially when Ca^{2+} is present at its binding site. It was reported by Jamal-Talabani *et al* [11] in 2004 as the first example of a calcium-dependent CBM. They used 1.6 M $MgSO_4$ solution to induce the crystallization and found two ion-binding sites in the CBM36 crystals (figure 1). The first ion-binding site, which binds Ca^{2+}, consists of the main chain carbonyls of Asp35 and Asp125 and the carboxylic oxygens of Asp125 and Glu16 side chains. The Ca^{2+} is also coordinated by a single water molecule. The second ion-binding site, which binds Mg^{2+}, consists of the main chain carbonyl of Tyr40 and the side chain carbonyl of Asp121, and four solvent water molecules (Protein Data Bank entry ID: 1w0n). In the presence of xylotriose and added Ca^{2+}, CBM36 forms a complex with xylotriose (Protein Data Bank entry ID: 1ux7). In this structure, Mg^{2+} in the second ion-binding site is replaced by Ca^{2+}, while the Ca^{2+} in first ion-binding site is conserved. The Ca^{2+} in the second ion-binding site is coordinated by the main chain carbonyl of Trp120, the side chain carboxyl of Asp116 and Asp121, a single water molecule, and two hydroxyl oxygens from xylotriose (hereafter, we call the ions in the first and second ion-binding site the *conserved* and *binding* ions, respectively, to distinguish them). Although the structure of the CBM36–xylotriose complex is well defined, the molecular mechanism of the ion dependencies of xylan-binding affinity is unclear.

In this paper, we examine the mechanism of selective binding of xylan by CBM36 and its ion species dependence through the combined use of molecular dynamics (MD) simulations and the 3D reference interaction site model (3D-RISM) method. In this approach, structure sampling of protein and ligand molecules is conducted using an MD simulation with explicit water molecules, which is followed by a solvation free energy calculation using the 3D-RISM method. In performing 3D-RISM calculations, the structure and coordinates of the protein and the ligand molecules, which are considered as 'solute molecules', are taken from MD snapshots, and all the explicit water molecules used in the MD simulation are omitted. For those solute molecules, the distribution of solvent water and solvation free energy are evaluated using the 3D-RISM method [12–14]. The advantage of this approach is that the thermodynamic properties of solvation with the complete ensemble average of an infinite number of solvent molecules can be obtained, and the fluctuation of the solute structure can be considered by the 3D-RISM method and MD simulation, respectively. This approach has been successfully applied to a variety of the molecular recognition processes of biomolecules, including CBMs [15–21]. In particular, Huang *et al* elucidated the role of water in the molecular recognition process of maltose-binding protein using 3D-RISM theory [20], which clearly shows its effectiveness.

In section 2, we describe the computational details and defined systems to which we applied the present approach. Section 3 shows the results of simulations, energy calculations, and solvation analysis. In section 4, we discuss the origin of the selective xylan binding and the role of Ca^{2+} at the binding site.

2. Computational methods

2.1. Structure sampling

For the structure sampling of CBM36, xylotriose, and their complex, we performed MD simulations under the isothermal–isobaric (NPT) ensemble. The x-ray crystal structure of the CBM36 complexed with xylotriose and Ca^{2+} (Protein Data Bank entry ID: 1ux7) was used for the initial geometry. The CBM36 complex was embedded in a rectangular water box of about $75 \times 90 \times 80$ Å^3 with a periodic boundary condition. One Na^+ was added to neutralize the system, and the total system consisted of about 53 000 atoms. To investigate the xylotriose-binding process and ion dependency of xylan-binding affinity, we constructed three similar systems: (1) the *binding* Ca^{2+} was replaced with Mg^{2+}, (2) xylotriose was removed, and (3) xylotriose was removed and the *binding* Ca^{2+} was replaced with Mg^{2+}. We also constructed a system consisting of xylotriose embedded in a rectangular water box of about $50 \times 50 \times 50$ Å^3. Thus, we conducted MD simulations of five systems in total. The Amber ff99SB-ILDN [22], GLYCAM06h [23], and TIP3P [24] force fields were used for the CBM36 protein, xylotriose, and water molecules, respectively. The ion–oxygen distance (IOD) set

of Lennard-Jones parameters developed by Li *et al* [25] was used for Mg^{2+} and Ca^{2+}.

We conducted equilibrium MD simulations for 10 ns, which were followed by 10 ns MD simulations for the data production. Long-range electrostatic interactions were treated with the particle mesh Ewald method. Bonds involving hydrogen atoms were constrained using the SHAKE method. The equations of motion were integrated using the leapfrog algorithm with an increment of 2 fs at 300 K and 1 bar. Two independent MD simulations were conducted for each system. The root-mean-square deviations of Cα atomic coordinates were about 1 Å during all the MD simulations, indicating that the CBM36 has a rigid backbone. However, in the system where Ca^{2+} was substituted with Mg^{2+}, CBM36 could not bind xylotriose during the MD simulations. We conducted three additional independent MD simulations, but the result was the same. The lack of binding indicates that CBM36 with bound Mg^{2+} has no xylan-binding affinity (see below also). Because CBM36 with bound Mg^{2+} could not bind xylotriose for more than 16 ns (10 ns for equilibration and 6 ns for sampling), the sampling MD simulation for 6 ns was used for further analysis. All the MD simulations were conducted using the AMBER 12 program package [26].

We also performed similar MD simulations with the Lennard-Jones parameters for Mg^{2+} and Ca^{2+} substituted with those developed by Åqvist [27]. However, even in the case of CBM36 with bound Ca^{2+}, all the trajectories did not reproduce the xylan-binding state. This result indicates that a force-field parameter for ions is essential to reproduce the nature of xylan binding. The difference between ion–water and ion–ligand interactions may be a key factor to determine the xylan-binding affinity. Therefore, the parameter set which appropriately reproduces the solvation structure of ions is required. The IOD parameter set is determined to reproduce the experimental values of the distance between ion and water oxygen and the coordination number of water. We therefore employed the IOD parameter set for all the analyses below.

2.2. Solvation free energy calculations

We employed the 3D-RISM method to evaluate the solvation free energy and the solvation structure of CBM36, xylotriose, and the CBM36–xylotriose complex. The solvation free energy was calculated for 1000 snapshots extracted every 10 ps from each trajectory (for the Mg^{2+}-bound CBM36–xylotriose complex system, 601 snapshots were used for the solvation free energy calculation). Here, all the explicit water molecules and the Na^{+} were omitted from the snapshots. The same potential parameters as in the MD simulation were employed for all the species. The temperature was 300 K and the density of solvent water was 1.0 g cm^{-3}. The grid points in the 3D-RISM calculations were 256^3, with a spacing of 0.5 Å. All the 3D-RISM calculations were conducted using the 3D-RISM code for the general-purpose GPU (GPGPU) developed by Maruyama and Hirata [28].

The free energy was calculated on the basis of the 3D-RISM and MD simulation by taking an ensemble average over the trajectory. Two trajectories were averaged individually with different initial conditions for each system. We employed trajectories that have lower averaged free energy in the following analysis.

3. Results and discussion

3.1. Xylan binding by CBM36

We now consider the process for xylotriose binding by CBM36 with bound Ca^{2+} to clarify the origin of the xylan-binding affinity at the molecular level. To analyze the process, we evaluated the free-energy difference between the xylotriose-binding and -unbinding states. The free-energy change for the xylotriose binding by CBM36 can be defined as

$$\Delta G = G^{\mathrm{complex}} - (G^{\mathrm{P\text{–}I}} + G^{\mathrm{X}}), \tag{1}$$

where G^{complex}, $G^{\mathrm{P\text{–}I}}$, and G^{X} denote the total free energy of the CBM36–ion–xylotriose complex, CBM36 with the *binding* ion, and xylotriose, respectively. The total free energy G can be decomposed into three components:

$$G = E_{\mathrm{conf}} + E_{\mathrm{int}} + \delta\mu, \tag{2}$$

where E_{conf}, E_{int}, and $\delta\mu$ are the conformational, intermolecular interaction, and solvation free energies, respectively. The solvation free energy is evaluated by the following formula within the framework of the 3D-RISM method:

$$\delta\mu = \rho k_{\mathrm{B}}T \sum_{\alpha\in\text{solvent site}} \int \left(\frac{1}{2} h_\alpha^2(\mathbf{r})\Theta(-h_\alpha(\mathbf{r})) - c_\alpha(\mathbf{r}) - \frac{1}{2} h_\alpha(\mathbf{r}) c_\alpha(\mathbf{r}) \right) \mathrm{d}\mathbf{r}, \tag{3}$$

where h_α and c_α denote the total and direct correlation functions for solvent site α. ρ, k_{B}, and T are the solvent number density, the Boltzmann constant, and the absolute temperature, respectively. Θ is the Heaviside step function. Here, we employed Kovalenko–Hirata closure to solve the 3D-RISM equation [13, 14, 29].

By substituting the free energies on the right-hand side of equations (1) with (2), equation (1) is rewritten as

$$\Delta G = \Delta E_{\mathrm{conf}} + \Delta E_{\mathrm{int}} + \Delta\delta\mu, \tag{4}$$

$$\Delta E_{\mathrm{conf}} = \Delta E_{\mathrm{conf}}^{\mathrm{P}} + \Delta E_{\mathrm{conf}}^{\mathrm{X}}, \tag{5}$$

and

$$\Delta E_{\mathrm{int}} = \Delta E_{\mathrm{int}}^{\mathrm{P\text{–}I}} + \Delta E_{\mathrm{int}}^{\mathrm{X\text{–}I}} + \Delta E_{\mathrm{int}}^{\mathrm{P\text{–}X}}, \tag{6}$$

where the superscripts P, I, and X mean the protein (CBM36), *binding* ion, and xylotriose, respectively. We note that the *conserved* Ca^{2+} is included in the protein term.

Table 1 summarizes the free-energy changes of xylotriose binding. In the case of CBM36 with bound Ca^{2+}, the xylotriose-binding free energy is −9.7 kcal mol^{-1}, which shows qualitative agreement with the experimental observation, −4.2 kcal mol^{-1}, although the value is overestimated [11]. The overestimation can be attributed to the force-field parameter set and the approximations inherent in the MD simulation and 3D-RISM method. The most important factor is the selection of the ion force field. Various models of ion force field have been proposed so far. We employ a simple non-bonded-type

Table 1. Free-energy change and its components for xylotriose binding to CBM with bound Ca^{2+} or Mg^{2+}.

Components	Ca^{2+}	Mg^{2+}
ΔG	−9.7 (1.5)	6.5 (1.7)
ΔE_{conf}	−8.8 (2.3)	−6.3 (3.3)
ΔE_{conf}^{P}	−11.4 (2.3)	−10.0 (3.3)
ΔE_{conf}^{X}	2.6 (0.3)	3.7 (0.3)
ΔE_{int}	−85.9 (0.9)	−92.9 (0.8)
ΔE_{int}^{P-I}	−19.1 (1.0)	−19.0 (0.8)
ΔE_{int}^{X-I}	−55.4 (0.4)	−57.8 (0.4)
ΔE_{int}^{P-X}	−11.3 (0.4)	−16.1 (0.4)
$\Delta\delta\mu$	85.0 (1.8)	105.8 (2.7)
ΔE_{uv}	174.5 (3.8)	218.6 (5.5)
ΔE_{vv}	−78.0 (1.8)	−95.9 (2.6)
$\Delta(-T\delta S_{solv})$	−11.6 (0.4)	−17.0 (0.5)

Note: Units are given in kcal mol^{-1}. The numbers in parentheses are the standard error.

model for the ion force field, where the interactions are represented by Coulombic and LJ terms in the model and all the other interactions, such as charge transfer, polarization and covalent interactions, are omitted. For more accurate results, therefore, an elaborated parameter set should be necessary [30]. However, the accuracy of the present force field is sufficient for our qualitative discussion on the ion dependency of xylan-binding affinity. In table 1, the statistical standard errors are also shown. The errors are small enough for the purposes of the discussion below. The changes of conformational and interaction energy, ΔE_{conf} and ΔE_{int}, show negative values, while that of the solvation free energy, $\Delta\delta\mu$, is positive. The value of ΔE_{int}, −85.9, is much lower than that of ΔE_{conf}, −8.8, which indicates that a major driving force of the xylan binding by CBM36 is attributed to the interaction between CBM36 and xylotriose. The interaction energy can be further decomposed into the contribution from the van der Waals and electrostatic interaction energies (table 2). The table shows that the electrostatic interaction between xylotriose and Ca^{2+} has a dominant contribution. Figure 2 depicts the averaged structure of the CBM36–xylotriose complex. Ca^{2+} is coordinated by the carboxyl oxygen of Asp116 and Asp121, the main chain carbonyl of Tyr40 and Trp120, and two hydroxyl oxygens of xylotriose. The electrostatic interactions between Ca^{2+} and the coordinated oxygens strongly contribute to the stabilization of the interaction energy between xylotriose and Ca^{2+}. The electrostatic interaction between ion and CBM36 is also stabilized by the xylotriose binding. This stabilization occurs because the distance between the carboxyl oxygen of Asp116 and Ca^{2+} becomes shorter due to the xylotriose binding (figure 3). Conversely, the van der Waals interaction is dominant in the interaction energy between CBM36 and xylotriose, ΔE_{int}^{P-X}. As can be seen in figure 4, one of the glucopyranose rings is stuck between the hydrophobic side chains of Tyr26 and Tyr40. We evaluated van der Waals interaction energy between xylotriose and Tyr26, and xylotriose and Tyr40. The energy is about −10.2 kcal mol^{-1}, which is the major contribution to the stabilization of the van der Waals interaction energy.

The solvation free energy change, $\Delta\delta\mu$, shows a largely positive value, which can be attributed intuitively to the dehydration penalty of CBM36, the *binding* ion, and xylotriose through making a complex. The solvation free energy, $\delta\mu$, can be decomposed into three terms, namely the solute–solvent interaction energy, E_{uv}, the solvent reorganization energy, E_{vv}, and the solvation entropy, $T\delta S_{solv}$ [31–33]:

$$\delta\mu = E_{uv} + E_{vv} - T\delta S_{solv}. \quad (7)$$

The solute–solvent interaction energy, E_{uv}, contributes to a positive value of $\delta\mu$, which results from the solvent water molecules on the xylan-binding surface being excluded by the steric hindrance of the complex formation. Table 3 shows the components of E_{uv}. Although all the components show positive values, the contribution of the ion is about twice that of the others. In figure 5, the distributions of the solvent water around the xylan-binding site are depicted. A conspicuous distribution can be found near Ca^{2+}, which corresponds to the coordinated water molecule suggested by the experiments [11]. The distribution of solvent becomes smaller by the complex formation with xylotriose. To compare the peak height of the solvent water, the radial distribution functions (RDFs) of water oxygen around the Ca^{2+} are depicted in figure 6. The first peak of the RDFs at 2.4 Å becomes lower by xylotriose binding. The diminished peak is a result of the coordination of the two hydroxyl oxygens of xylotriose to Ca^{2+} instead of the solvent water. By contrast, the solvation entropy and the solvent reorganization terms in table 1 are negative, because the solvent water molecules on the xylan-binding surface are released from hydrophilic interaction with the ion, CBM36, and xylotriose.

3.2. Ion dependency of xylan-binding affinity

CBM36 binds Mg^{2+} at the xylan-binding site in the absence of xylotriose and in the presence of 1.6 M $MgSO_4$, although Ca^{2+} binding takes place in the presence of xylotriose and added Ca^{2+}. In this subsection, we consider the mechanism of the ion selectivity of CBM36 and its effects on xylan binding.

To consider the ion selectivity of CBM36 at the xylan-binding site, the free-energy change by Ca^{2+} substitution with Mg^{2+}, ΔG^{Mg-Ca}, is evaluated, and is defined as:

$$\Delta G^{Mg-Ca} = (G^{P(Mg)} + G^{Ca}) - (G^{P(Ca)} + G^{Mg}), \quad (8)$$

where $G^{P(Mg)}$ and G^{Ca} denote the free energies of CBM36 with bound Mg^{2+} and Ca^{2+} in water, respectively. ΔG^{Mg-Ca} can be split into three components, namely the change in structural energy of the protein, interaction energy between the protein and ion, and solvation free energy:

$$\Delta G^{Mg-Ca} = \Delta E_{conf}^{P} + \Delta E_{int}^{P-I} + \Delta\delta\mu. \quad (9)$$

Table 4 summarizes the free-energy change and its components by the ion replacement from Ca^{2+} with Mg^{2+}. The results show that CBM36 has a slightly greater affinity for Ca^{2+} than Mg^{2+} in water. The solvation free energy change

Table 2. Components of the interaction energy change after xylotriose binding to CBM with bound Ca^{2+} or Mg^{2+}.

	Ca^{2+}			Mg^{2+}		
Components	ΔE_{int}^{P-I}	ΔE_{int}^{X-I}	ΔE_{int}^{P-X}	ΔE_{int}^{P-I}	ΔE_{int}^{X-I}	ΔE_{int}^{P-X}
vdW	3.1	3.6	−20.9	−1.8	2.0	−21.2
	(0.2)	(0.1)	(0.1)	(0.2)	(0.1)	(0.1)
ES	−22.2	−59.0	9.6	−17.3	−59.8	5.2
	(1.0)	(0.4)	(0.4)	(0.9)	(0.4)	(0.4)

Note: vdW and ES denote the van der Waals and electrostatic interaction energies, respectively. Units are given in kcal mol^{-1}. The numbers in parentheses are the standard error.

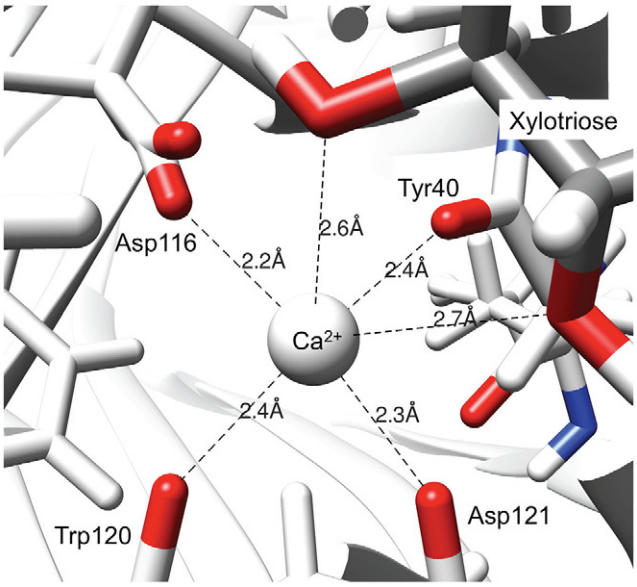

Figure 2. Averaged structures of the CBM36–xylotriose complex around the xylan-binding site with Ca^{2+}.

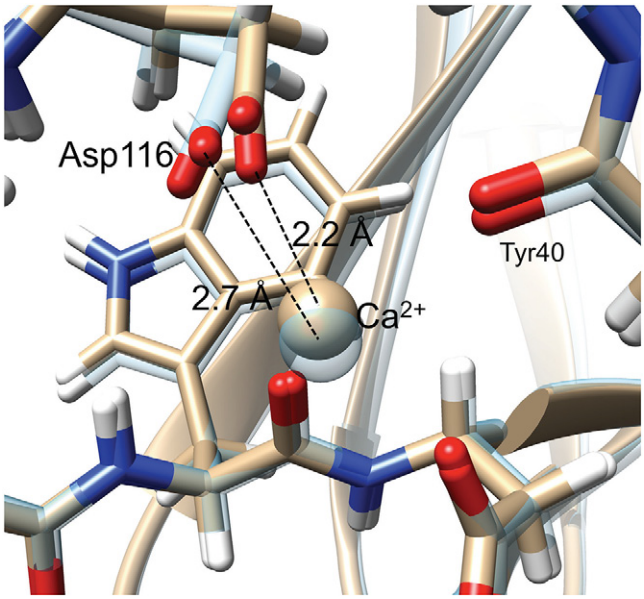

Figure 3. Structural change of the averaged structures of the CBM36–xylotriose complex around the xylan-binding site with Ca^{2+}. Green and white colored backbones are the binding and unbinding states of CBM36, respectively.

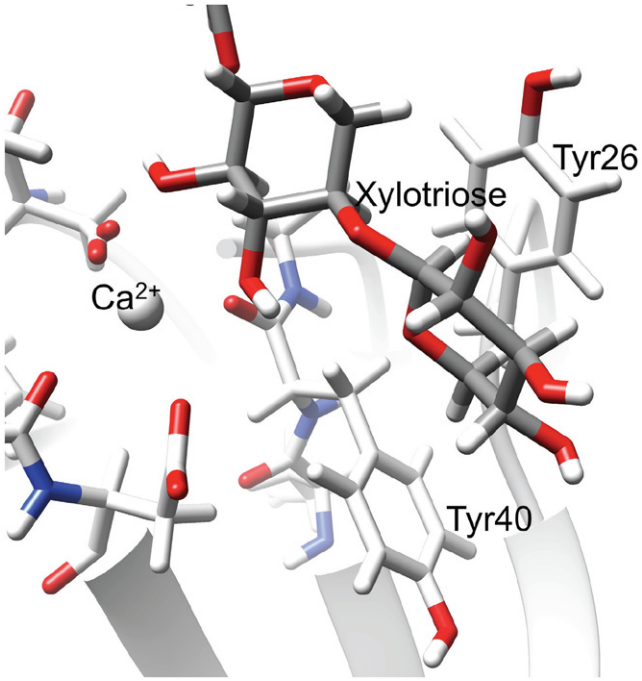

Figure 4. Close-up view of xylotriose, Tyr40, and Tryr26 of the averaged structures of the CBM36–xylotriose complex.

Table 3. Components of the solute–solvent interaction energy change after xylotriose binding to CBM with bound Ca^{2+} or Mg^{2+}.

Components	Ca^{2+}	Mg^{2+}
ΔE_{uv}^{P}	41.3 (3.7)	67.1 (5.7)
ΔE_{uv}^{I}	85.3 (1.0)	99.4 (0.9)
ΔE_{uv}^{X}	47.8 (0.4)	52.2 (0.4)

Note: Units are given in kcal mol^{-1}. The numbers in parentheses are the standard error.

shows large positive values because Mg^{2+} should pay a higher dehydration penalty than the stabilization of the Ca^{2+} hydration. By contrast, protein–ion interaction is strongly stabilized by the Mg^{2+} binding, because the distances between Mg^{2+} and the coordinated residues are shorter than those for Ca^{2+} (figure 7). These structural changes may make the protein structure unstable. The dehydration penalty of Mg^{2+} and the enhancement of the protein–ion interaction energy are almost canceled out by each other. As a result, the total free-energy

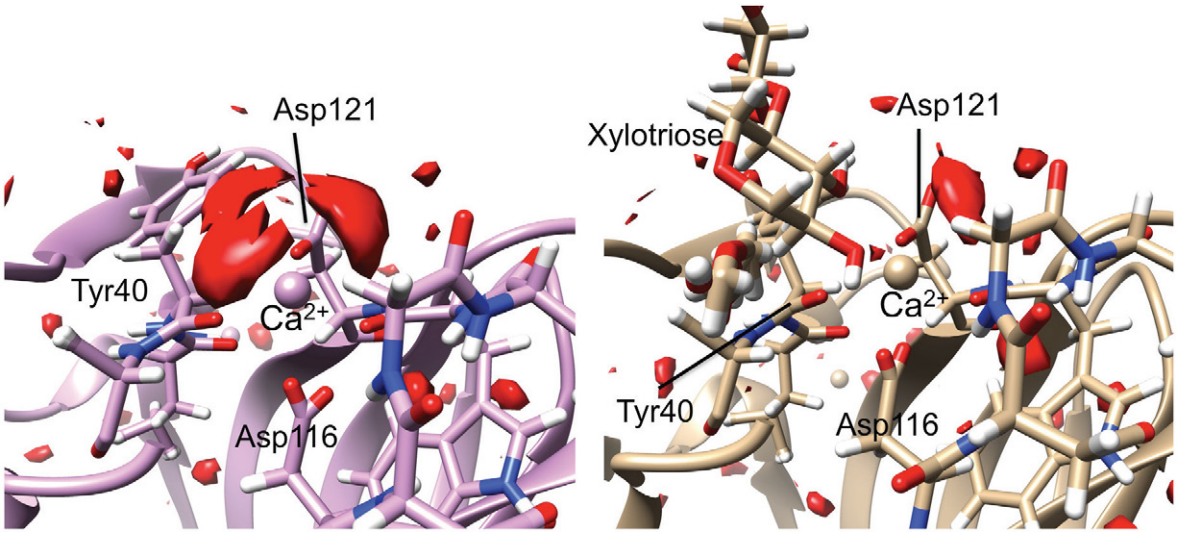

Figure 5. Isosurface plot of the averaged water distribution around the xylan-binding site of unbinding (left) and binding (right) states (isovalue = 3.0).

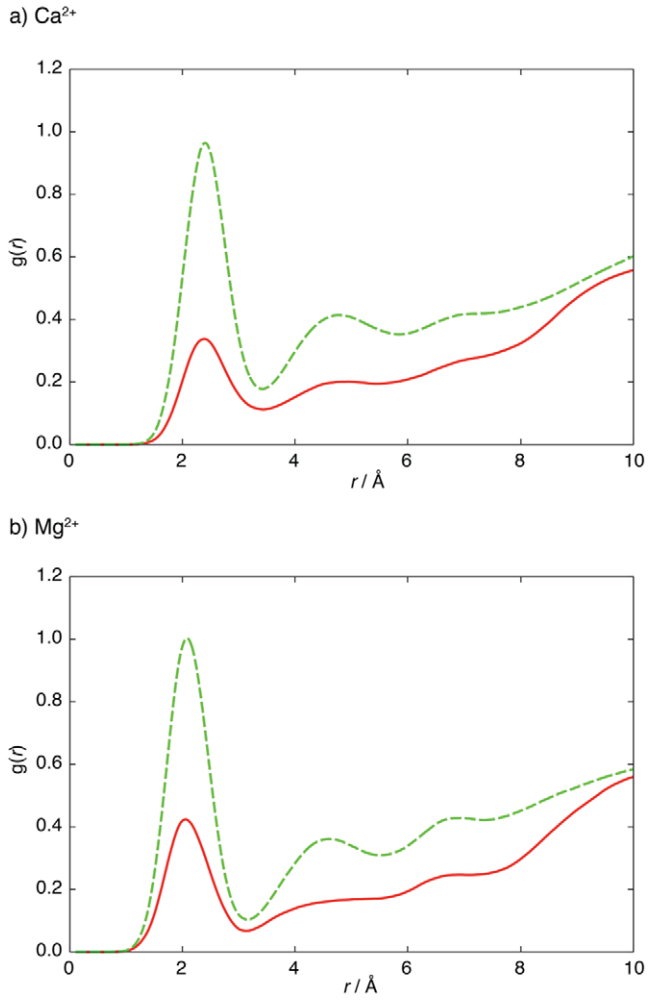

Figure 6. Radial distribution of the solvent water oxygen around (a) Ca^{2+} and (b) Mg^{2+} at the binding site. Solid and dashed lines denote the binding and unbinding states, respectively.

change due to the ion replacement by Ca^{2+} with Mg^{2+} is only 4.0 kcal mol^{-1}. This indicates that CBM36 preferably binds Ca^{2+} rather than Mg^{2+}, but it can bind the Mg^{2+} in an environment of high Mg^{2+} concentration. This result is consistent with experimental observations [11].

Table 4. Free-energy change and its components due to ion replacement from Ca^{2+} to Mg^{2+}.

Components	
$\Delta G^{\mathrm{Mg-Ca}}$	4.0 (1.4)
$\Delta E^{\mathrm{P}}_{\mathrm{conf}}$	10.8 (2.4)
$\Delta E^{\mathrm{P-I}}_{\mathrm{int}}$	−74.4 (0.8)
$\Delta\delta\mu$	67.6 (1.7)

Note: The numbers in parentheses are the standard error.

To understand the difference in the affinity of binding for xylan by CBM36s with bound Ca^{2+} or Mg^{2+}, the free-energy components for the xylan-binding process of both scenarios are summarized in table 1. Where CBM36 binds Mg^{2+}, the binding free energy, 6.5 kcal mol^{-1}, is positive, which means that the CBM36 with bound Mg^{2+} has no affinity for xylan. This result is consistent with the MD simulation. All the components for the CBM36 with bound Mg^{2+} are similar to those for the CBM36 with bound Ca^{2+}. The difference in the conformational energy change is only 2.5 kcal mol^{-1} and that of the interaction energy is 7 kcal mol^{-1}. As can be seen from table 2, the components of the interaction energy show only small differences. However, the solvation free energy term shows a dramatic change when Ca^{2+} is replaced by Mg^{2+}: the difference is 20.8 kcal mol^{-1}. Such a dramatic change is attributed to the stronger Mg^{2+}–water interaction compared with that for Ca^{2+}, as discussed above. In figure 6, the RDFs of the solvent water oxygen around the *binding* ions are depicted. The first RDF peaks appear at 2.4 Å for Ca^{2+} and 2.1 Å for Mg^{2+}. In both cases, the peaks are attenuated by the formation of a complex with xylotriose. Therefore, Mg^{2+} should pay a higher dehydration penalty due to the complex formation because of the stronger interaction between the ion and water than in the case of Ca^{2+}. This explains the larger change in *binding* ion–solvent interaction energy change, $\Delta E^{\mathrm{I}}_{\mathrm{uv}}$. The

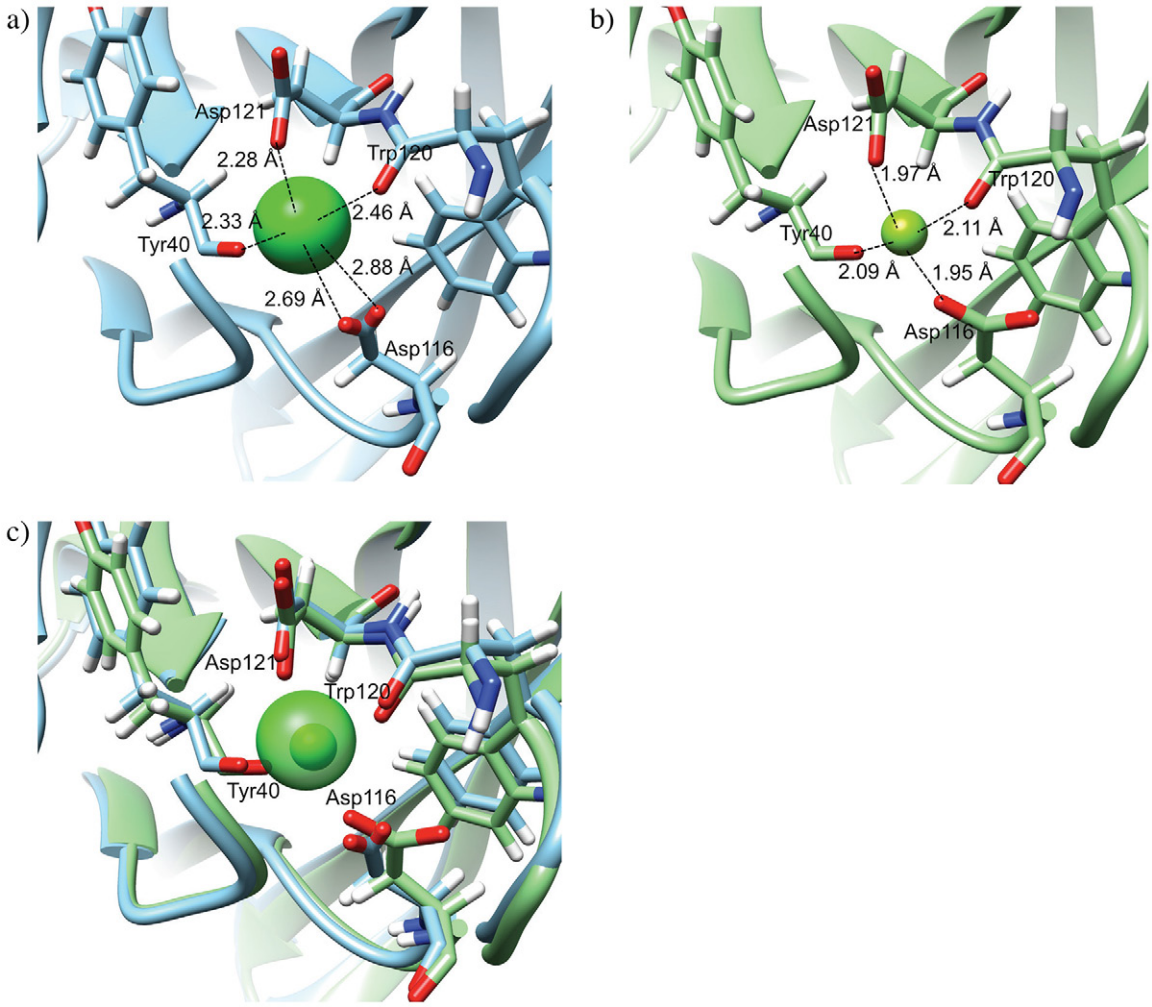

Figure 7. Averaged structures of CBM36 around the xylan-binding site with (a) Ca^{2+} and (b) Mg^{2+}. The superposition description of two structures is shown in (c).

other components of the solute–solvent interaction energy of CBM36 with bound Mg^{2+}, namely ΔE^{P}_{uv} and ΔE^{X}_{uv}, also show greater change than those in the CBM36 with bound Ca^{2+}. The change may be attributed to the greater solvation structure change due to the complex formation when CBM is bound to Mg^{2+} rather than Ca^{2+}.

These results suggest that the affinity of CBM36 for xylan is achieved by a balance of the interactions between the binding ion and solvent, hydrophilic residues around xylan, and hydroxyl oxygens of xylan. Where CBM36 is bound to Mg^{2+}, the dehydration penalty of Mg^{2+} is too large to compensate for the energy of interaction with xylan.

4. Conclusion

The mechanism of the binding of CBM36 to xylan and the role of Ca^{2+} are investigated theoretically by the combined use of MD simulation and the 3D-RISM method. We found that CBM36 with bound Ca^{2+} has an affinity for xylan while CBM36 with bound Mg^{2+} has no such affinity. The free-energy component analysis of the xylan-binding process revealed that the major factor in the xylan-binding affinity is the electrostatic interaction with Ca^{2+} and the hydroxyl oxygens of xylan. The van der Waals interaction between the hydrophobic side chain of CBM36 and the glucopyranose ring of xylan also contributes to the stabilization of the xylan-binding state. Dehydration of the complex formation opposes these interactions. Therefore, the affinity of CBM36 for xylan is achieved by a balance of the interactions between the binding ion and the solvent, hydrophilic residues around xylan, and hydroxyl oxygens of xylan. Where CBM36 is bound to Ca^{2+}, these factors are well balanced and the total free-energy change on binding xylan is negative. By contrast, because CBM36 with bound Mg^{2+} shows a larger dehydration penalty upon binding, it has no affinity for xylan.

We have elucidated the details of CBM36 binding with xylan at a molecular level. A deeper understanding of the mechanism can lead to useful knowledge, for example, about how to make a mutant that has different ion and carbohydrate affinities. The results of the present study should contribute to the design of highly efficient CBM36 and control of its selectivity for various polysaccharides.

Acknowledgments

We are grateful to Dr Maruyama for providing the 3D-RISM code suitable for the GPGPU [28]. Numerical calculations were conducted in part at the Research Center for Computational Science, Institute for Molecular Science, and National Institutes of Natural Sciences in Japan. We thank the Next-Generation Supercomputing Project, Nanoscience Program and the strategic programs for innovative research (SPIRE) and the computational materials science initiative (CMSI), Japan for their support. This work was supported by the Kyushu University Interdisciplinary Programs in Education and Projects in Research Development, and Grants-in-Aid (25410021, 26104526, 15K05392, 16H00842, 16K05519, 26810008, 16H00778) from MEXT, Japan.

References

[1] Gilkes N R, Henrissat B, Kilburn D G, Miller R C Jr and Warren R A 1991 *Microbiol. Rev.* **55** 303–15
[2] Henrissat B and Davies G J 2000 *Plant Physiol.* **124** 1515–9
[3] Bolam D N, Ciruela A, McQueen-Mason S, Simpson P, Williamson M P, Rixon J E, Boraston A, Hazlewood G P and Gilbert H J 1998 *Biochem. J.* **331** 775–81
[4] Din N, Damude H G, Gilkes N R, Miller R C Jr, Warren R A and Kilburn D G 1994 *Proc. Natl Acad. Sci. USA* **91** 11383–7
[5] Gilbert H J, Knox J P and Boraston A B 2013 *Curr. Opin. Struct. Biol.* **23** 669–77
[6] Van Tilbeurgh H, Tomme P, Claeyssens M, Bhikhabhai R and Pettersson G 1986 *FEBS Lett.* **204** 223–7
[7] Kraulis J, Clore G M, Nilges M, Jones T A, Pettersson G, Knowles J and Gronenborn A M 1989 *Biochemistry* **28** 7241–57
[8] Charnock S J, Bolam D N, Nurizzo D, Szabo L, McKie V A, Gilbert H J and Davies G J 2002 *Proc. Natl Acad. Sci. USA* **99** 14077–82
[9] van Bueren A L, Morland C, Gilbert H J and Boraston A B 2005 *J. Biol. Chem.* **280** 530–7
[10] Boraston A B, McLean B W, Kormos J M, Alam M, Gilkes N R, Haynes C A, Tomme P, Kilburn D G and Warren R A J 1999 Carbohydrate-binding modules: diversity of structure and function *Recent Adv. Carbohyd. Bioeng.* ed B Svensson (Cambridge: Royal Society of Chemistry) pp 202–11
[11] Jamal-Talabani S, Boraston A B, Turkenburg J P, Tarbouriech N, Ducros V M and Davies G J 2004 *Structure* **12** 1177–87
[12] Beglov D and Roux B 1997 *J. Phys. Chem.* B **101** 7821–6
[13] Kovalenko A and Hirata F 1999 *J. Chem. Phys.* **110** 10095–112
[14] Kovalenko A and Hirata F 1998 *Chem. Phys. Lett.* **290** 237–44
[15] Phanich J, Rungrotmongkol T, Sindhikara D, Phongphanphanee S, Yoshida N, Hirata F, Kungwan N and Hannongbua S 2016 *Protein Sci.* **25** 147–58
[16] Blinov N, Dorosh L, Wishart D and Kovalenko A 2010 *Biophys. J.* **98** 282–96
[17] Luchko T, Gusarov S, Roe D R, Simmerling C, Case D A, Tuszynski J and Kovalenko A 2010 *J. Chem. Theory Comput.* **6** 607–24
[18] Genheden S, Luchko T, Gusarov S, Kovalenko A and Ryde U 2010 *J. Phys. Chem.* B **114** 8505–16
[19] Yui T, Shiiba H, Tsutsumi Y, Hayashi S, Miyata T and Hirata F 2010 *J. Phys. Chem.* B **114** 49–58
[20] Huang W, Blinov N, Wishart D S and Kovalenko A 2015 *J. Chem. Inf. Model.* **55** 317–28
[21] Yoshida N, Imai T, Phongphanphanee S, Kovalenko A and Hirata F 2009 *J. Phys. Chem.* B **113** 873–86
[22] Lindorff-Larsen K, Piana S, Palmo K, Maragakis P, Klepeis J L, Dror R O and Shaw D E 2010 *Proteins Struct. Funct. Bioinf.* **78** 1950–8
[23] Kirschner K N, Yongye A B, Tschampel S M, Gonzalez-Outeirino J, Daniels C R, Foley B L and Woods R J 2008 *J. Comput. Chem.* **29** 622–55
[24] Jorgensen W L, Chandrasekhar J, Madura J D, Impey R W and Klein M L 1983 *J. Chem. Phys.* **79** 926–35
[25] Li P, Roberts B P, Chakravorty D K and Merz K M Jr 2013 *J. Chem. Theory Comput.* **9** 2733–48
[26] Case D A *et al* 2012 *AMBER12* (San Francisco, CA: University of California)
[27] Aqvist J 1990 *J. Phys. Chem.* **94** 8021–4
[28] Maruyama Y and Hirata F 2012 *J. Chem. Theory Comput.* **8** 3015–21
[29] Kovalenko A and Hirata F 1999 *J. Phys. Chem.* B **103** 7942–57
[30] Project E, Nachliel E and Gutman M 2008 *J. Comput. Chem.* **29** 1163–9
[31] Yu H A and Karplus M 1988 *J. Chem. Phys.* **89** 2366–79
[32] Yu H A, Roux B and Karplus M 1990 *J. Chem. Phys.* **92** 5020
[33] Imai T, Harano Y, Kinoshita M, Kovalenko A and Hirata F 2006 *J. Chem. Phys.* **125** 024911